Interdisciplinary Research in Medical Sciences Specialty
ISSN: 3062-4401
2026, Volume 6, Issue 1, Page No: 58-71

Available online at: www.galaxypub.co/page/journals

Galaxy Publication

A Gold Nanoparticle Spherical Nucleic Acid Probe for In Situ Detection of Exosomal and Cellular piR-651 in Cancer Diagnosis

Ahmed Ben Ali[1]*, Samira Gharbi[1], Nabil Jebali[2]

[1]Department of Nanodiagnostics and Cancer Detection, Faculty of Medicine, University of Tunis, Tunis, Tunisia.
[2]Department of Exosomal Biomarkers and Gold Nanoparticles, Faculty of Medicine, University of Sfax, Sfax, Tunisia.

***E-mail** ✉ ahmed.benali@fpharm.u-tunis.tn

Received: 08 February 2026; **Revised:** 18 April 2026; **Accepted:** 24 April 2026

ABSTRACT

A growing body of research indicates that PIWI-interacting RNAs (piRNAs) encapsulated in circulating exosomes represent promising novel molecular biomarkers suitable for tumor liquid biopsy. Nonetheless, available techniques for the direct in situ identification of exosomal piRNAs are still inadequate. Here, we developed a spherical nucleic acid-based probe called piR-651 that readily enters exosomes after a 2 h incubation period and permits in situ detection of piR-651 with a limit of detection of 5×10^7 particles/μL. Using this probe, we devised a liquid biopsy strategy enabling the in situ analysis of piR-651 in plasma-derived exosomes. The developed assay successfully differentiated piR-651 expression between plasma samples from 21 breast cancer patients and 22 healthy volunteers. Analysis of the receiver operating characteristic curve revealed an area under the curve of 0.9931, while the optimal cutoff value provided a diagnostic sensitivity of 85.7% and specificity of 100%. In addition, the probe supports convenient in situ visualization of piR-651 within living cells. To address the challenges of reduced sensitivity and slow reaction kinetics associated with detecting bulky PIWI-interacting RNA complexes, we carefully optimized both the architecture and operational mechanism of the piR-651 probe. The probe was fabricated by conjugating high-density Anchor-Report DNA duplexes onto 13-nm gold nanoparticles using the butanol dehydration approach. This innovative gold nanoparticle nucleic acid probe design can be extended to create probes for other large-volume nucleic acid targets, thereby facilitating the advancement of further liquid biopsy platforms reliant on molecular biomarkers for cancer diagnosis.

Keywords: Breast cancer diagnosis, In situ detection, piR-651, Plasma exosomes, Spherical nucleic acid

How to Cite This Article: Ben Ali A, Gharbi C, Jebali N. A Gold Nanoparticle Spherical Nucleic Acid Probe for In Situ Detection of Exosomal and Cellular piR-651 in Cancer Diagnosis. Interdiscip Res Med Sci Spec. 2026;6(1):58-71. https://doi.org/10.51847/73tr1oo0IF

Introduction

The latest statistics released by the World Health Organization (WHO) indicate that breast cancer affects approximately 2.3 million individuals globally each year, corresponding to 11.6% of all new cancer diagnoses and placing it second only to lung cancer in incidence [1]. Common screening approaches for breast cancer include breast ultrasound, mammography, and magnetic resonance imaging [2]. Despite their widespread clinical application, these techniques have important drawbacks. Mammography, for example, performs less effectively in younger women who generally possess denser breast tissue or in tumors with certain molecular characteristics. Additionally, the procedure exposes patients to radiation and causes significant discomfort, which negatively affects screening compliance and may result in overlooked cases and postponed therapeutic intervention. Hence, the establishment of simple, well-tolerated, accurate, and sensitive methods for breast cancer screening is of critical importance. Liquid biopsy involves the analysis of tumor-derived materials such as circulating tumor cells (CTCs), circulating tumor DNA (ctDNA), extracellular vesicles (EVs), and other components shed into bodily fluids using non-invasive in vitro assays [3-6], thereby supporting early diagnosis and therapeutic decision-making

in oncology. The molecular contents of EVs—including proteins, microRNAs, piwi-interacting RNAs (piRNAs), and mRNAs—mirror the physiological condition of tumor cells and open new possibilities for cancer molecular diagnostics [7, 8].

Although miRNAs in cellular and exosomal compartments have been extensively studied, the contributions of piRNAs to disease pathogenesis and diagnosis have received comparatively less attention. PIWI-interacting RNAs (piRNAs) are a distinct group of small non-coding RNAs, ranging from 21 to 35 nucleotides in length, that interact with the PIWI subfamily of Argonaute proteins [9-11]. These RNAs are vital for genomic stability, exerting effects through transposon silencing, telomere complex stabilization, and epigenetic control of gene expression [12-14]. Accumulating evidence demonstrates that altered piRNA expression levels play significant roles in disease initiation and advancement [15, 16]. Notably, several dysregulated piRNAs, including piR-36712, piR-651, piR-021285, and piR-932, have been associated with breast cancer [17]. In particular, piR-651 promotes breast cancer cell proliferation and migration while reducing apoptosis by enhancing DNMT1-dependent methylation of the PTEN promoter, highlighting its potential value as both a diagnostic biomarker and a therapeutic target [18].

Existing methods for piRNA detection predominantly depend on microarray hybridization, quantitative real-time polymerase chain reaction, and next-generation sequencing, although several innovative biosensing platforms have recently emerged. Lee *et al*. reported a molecular beacon probe targeting piR-36026 that enabled single-cell imaging of this highly expressed piRNA in MCF-7 breast cancer cells and suppressed its tumor-promoting activity [19]. Jia *et al*. constructed aptamer-modified activatable DNA tetrahedral nanoprobes capable of imaging and controlling endogenous piRNAs in cancer cells, thus providing new tools for breast cancer management [20]. Our research group has recently concentrated on developing sensitive analytical techniques for exosomal piRNAs in plasma and their integration into liquid biopsy workflows. These include a universal catalytic hairpin self-assembly system [21], multiple enzyme-free isothermal amplification strategies performed in butanol-water biphasic media [22], and an ultrasensitive split DNAzyme assay facilitated by butanol dehydration [23]. A major drawback of these approaches is the requirement for exosome disruption and proteinase K treatment to dismantle PIWI protein-piRNA complexes prior to analysis, which adds considerable time and complexity. Therefore, a straightforward in situ detection strategy for exosomal piRNAs is urgently needed.

Gold nanoflares have previously been employed by our team and other researchers for the in situ detection and imaging of miRNAs inside exosomes [24-26] and could theoretically be adapted for piRNA analysis. However, although piRNAs differ from miRNAs by only about 10 nt, their association with 97 kD PIWI proteins results in large macromolecular complexes that create substantial steric barriers for traditional nanoflare probes. To overcome this limitation, the current study presents a rationally designed gold nanoparticle-cored spherical nucleic acid probe named the piR-651 probe, tailored for the in situ detection of piR-651 within exosomes. Both the probe structure and detection workflow were specifically engineered to accommodate large PIWI-interacting RNA complexes, minimizing steric hindrance while preserving analytical sensitivity. Employing this probe, we established a highly accurate liquid biopsy method centered on the quantification of plasma exosomal piR-651 for breast cancer diagnosis. The probe also enabled successful in situ imaging of piR-651 expression in living single cells.

Materials and Methods

Experimental instruments and materials

All HPLC-purified oligonucleotide sequences and the 4-(2-Hydroxyethyl)-1-piperazineethanesulfonic acid (HEPES, pH = 7.6) buffer solution were commercially obtained from Shanghai Sangon Biotech Co. Ltd., China. Hydrogen tetrachloroaurate (III) trihydrate ($HAuCl_4 \bullet 3H_2O$) was purchased from Shanghai Aladdin Bio-Chem Technology Co. Ltd., China. Trisodium citrate dihydrate ($C_6H_5Na_3O_7 \bullet 2H_2O$) came from Guangzhou Chemical Reagent Factory, China. Fetal bovine serum (FBS) was supplied by Wuhan Punoasis Life Science & Technology Co., China. The antibiotic-containing cell culture medium was provided by Jiangsu Kaiji Biotechnology Co., China. Both the MCF-7 breast cancer cell line and the MCF-10A normal human breast epithelial cell line were acquired from the cell collection maintained by the School of Pharmaceutical Sciences at Southern Medical University, China. Clinical plasma specimens were obtained from China Southern Hospital of Southern Medical University and Shenzhen Baoan District Shiyan People's Hospital following appropriate informed consent procedures.

Exosomes secreted by cultured cells were isolated and refined using a high-speed centrifuge (model HC-2062, Hunan Herexi Instrument Co.) combined with a Beckman ultracentrifuge (Optima XPN-100, Beckman Coulter Life Sciences Inc.). Particle size distribution and concentration of the purified exosomes were measured with a nanoparticle tracking analyzer (Zeta View Particles Metrix). Fluorescence signals were quantified using a multifunctional microplate reader (Infinite M1000, Tecan). Morphological characterization of the gold nanoparticles and assembled piR-651 probe was performed on a HITACH H-7650 transmission electron microscope (Japan).

Synthesis and characterization of the piR-651 probe

Monodisperse 13 nm gold nanoparticles (AuNPs) were initially prepared through the conventional citrate-mediated reduction of chloroauric acid [27] (detailed procedures are provided in the ESI). The functional piR-651 probe was subsequently constructed by anchoring high-density oligonucleotide duplexes onto the AuNP surface via the accelerated butanol dehydration protocol [28]. In a typical preparation, Anchor DNA and Report DNA **(Table 1)** were each prepared at 92 μM, with 1.5 μL of each strand combined at a 300:1 molar ratio to AuNPs. The mixture was heated to 95°C for 5 min to denature the strands and then allowed to cool gradually to room temperature to promote complete hybridization. Following this, 46 μL of 10 nM AuNP colloid and 1 μL of 750 mM NaCl solution were added to bring the total volume to 50 μL. Next, 450 μL of n-butanol was introduced, and the system was vortexed for 8–9 s until a clear, transparent solution formed. Immediately after, 100 μL of 0.5 × TBE buffer was added with further vortexing for 9 s. The resulting mixture underwent brief centrifugation at 2000 g for 5 s, producing a red precipitate at the tube base. This precipitate was transferred to a fresh 1.5 mL EP tube and pelleted by centrifugation at 15,000 rpm for 15 min at 4°C. After removing the supernatant, the pellet was washed three successive times with 46 μL of 25 mM HEPES buffer (containing 100 mM NaCl, pH = 7.6) using identical centrifugation parameters (15,000 rpm, 4°C, 15 min). Finally, the purified material was resuspended in 46 μL of 25 mM HEPES solution. All synthetic steps were carried out with protection from light.

Table 1. Sequences of the oligonucleotide chains immobilized on the piR-651 probe, piR-651 nanoflare, and piR-16926 probe.

Name	Sequence (5′–3′)
Anchor DNA on piR-651 probe	CCCGTGCCTTGGAAAGCGTC$(A)_7$-SH
Report DNA on piR-651 probe	Cy5-GACGCTTTCCAAGGCACGGGCCCCTCTCT
Capture DNA on piR-651 nanoflare	GACGCTTTCCAAGGCACGGGCCCCTCTCT$(A)_7$-SH
Report DNA on piR-651 nanoflare	Cy5-CCCGTGCCTTGGAAAGCGTC
Anchor DNA on piR-16926 probe	TGCTGGGCCCATAACCCAGA$(A)_7$-SH
Report DNA on piR-16926 probe	Cy5-TCTGGGTTATGGGCCCAGCACGCTTCCG
piR-651	AGAGAGGGGCCCGUGCCUUGGAAAGCGUC
piR-16926	CGGAAGCGUGCUGGGCCCAUAACCCAGA

Characterization of the prepared piR-651 probe included several analytical techniques: UV-Vis absorption spectra were scanned from 400 to 700 nm to establish peak positions and calculate probe concentration; hydrodynamic diameter and size distribution were determined by dynamic light scattering (DLS); surface charge was evaluated via Zeta potential analysis; and detailed particle morphology and core dimensions were visualized by transmission electron microscopy (TEM).

For comparison purposes, a structurally related negative control probe (piR-16926 probe) designed to target piR-16926, as well as a classical nanoflare architecture probe for piR-651 detection (piR-651 nanoflare) [29], were synthesized following the identical butanol dehydration procedure. The complete set of oligonucleotide sequences employed for surface modification is summarized in **Table 1**.

Determination of DNA loading on the piR-651 probe

DNA surface density on the piR-651 probe was quantified through a standard addition technique. A set of reaction mixtures was prepared, each containing 0.5 nM of the piR-651 probe along with 40 mM tris-(2-carboxyethyl)-phosphine (TCEP) and Anchor DNA-Report DNA duplexes at concentrations varying from 0 to 120 nM, brought to a total volume of 50 μL with HEPES buffer. These solutions were allowed to incubate at ambient temperature

while shielded from light for 30 min. Fluorescence emission from each mixture was then recorded on a multifunctional microplate reader (excitation: 640 nm; emission: 665 nm). The resulting intensity values were plotted versus duplex concentration, and linear regression analysis of the data enabled calculation of the DNA loading level on the probe.

Determination of anti-DNase I stability of the piR-651 probe

The ability of the piR-651 probe to withstand DNase I degradation was evaluated by mixing 0.5 nM probe with varying amounts of DNase I (final concentrations of 0 to 500 U/mL) in 50 μL volumes within a 384-well plate. After incubation for 1 h at room temperature in darkness, fluorescence intensity was measured using a multifunctional microplate reader (excitation wavelength 640 nm, emission wavelength 665 nm). Ratios of sample fluorescence to background signal were graphed as a function of enzyme concentration. Equivalent mixtures containing the probe and DNase I were additionally supplemented with 1.5 mg/mL EDTA (final concentration) and subjected to the identical incubation and measurement protocol to examine the influence of EDTA on probe stability against enzymatic digestion.

Detection of piR-651 in the solution

Analytical performance of the probe toward free target in buffer was assessed by combining 0.5 nM piR-651 probe with piR-651 at concentrations ranging from 0 to 50 nM in 50 μL HEPES buffer per well of a 384-well plate. Mixtures were incubated at room temperature protected from light for 1 h. Fluorescence intensity was subsequently measured on a multifunctional microplate reader (excitation 640 nm, emission 665 nm). The relationship between signal-to-background ratio (S/B) and target concentration was plotted to determine detection capability in solution.

Determination of the selectivity of the piR-651 probe to nucleic acids

To evaluate specificity, 0.5 nM piR-651 probe was incubated individually with 20 nM concentrations of the authentic piR-651 sequence, DNA versions of miR-1246 and miR-21, or several random DNA oligonucleotides **(Table 2)** in 50 μL HEPES buffer. Incubations occurred at room temperature in the dark for 1 h. A probe-only control without any target nucleic acid was prepared in parallel. Fluorescence intensities were recorded for all samples using a multifunctional microplate reader (excitation 640 nm, emission 665 nm). A bar graph of the resulting signal-to-background ratios (S/B) for each nucleic acid type was generated to illustrate probe selectivity.

Table 2. DNA sequences applied in the selectivity evaluation of the piR-651 probe.

Name	Sequence (5′–3′)
miR-21 analog	TAGCTTATCAGACTGATGTTGA
miR-1246 analog	AATGGATTTTTGGAGCAGG
Random DNA-1	AGAGAGGGCCCCGTGCCTTGGAAAGCGTC
Random DNA-2	AGAGAGGGCCCCGTGCCTGGGAAAGCGTC
Random NDA-3	AGAGAGGGCCCCGAGCCTGGGAAAGCGTC

Note: Bases marked by underlining in the Random DNAs represent positions that differ from the matching sites in the piR-651 sequence.

Isolation, extraction, and identification of exosomes

MCF-7 and MCF-10A cells were maintained in 10-cm dishes at 37°C under a 5% CO_2 atmosphere. Culture conditions for MCF-7 cells utilized DMEM medium containing 10% fetal bovine serum (FBS) and 1% penicillin-streptomycin. MCF-10A cells were propagated in a dedicated medium based on DMEM/F12 (1:1) supplemented with 5% horse serum, 10 μg/mL insulin, 20 mg/mL epidermal growth factor, 100 ng/mL cholera toxin, and 0.5 μg/mL hydrocortisone. Once cells achieved 50%–60% confluence, the growth medium was substituted with DMEM containing 10% exosome-depleted FBS, and cultivation proceeded until cells reached roughly 90% confluence. Culture supernatants were collected, and exosomes were purified by differential centrifugation performed at 4°C. This process included successive spins at 300 × g for 10 min, 2000 × g for 20 min, and 10,000 × g for 30 min to clear residual intact cells, apoptotic bodies, and debris. The cleared supernatant underwent ultracentrifugation at 110,000 × g for 70 min at 4°C. The collected pellet was rinsed with PBS and subjected to a

second ultracentrifugation step at 110,000 × g for 80 min at 4°C. Following supernatant removal, the exosome pellet was resuspended in 100 μL of PBS and kept at −80°C for subsequent experiments.
Exosome characterization included the following analyses: particle concentration and size distribution were assessed using nanoparticle tracking analysis (NTA); morphology and diameter were visualized by transmission electron microscopy (TEM); and signature exosomal proteins were confirmed via Western blot (WB) (additional procedural information is available in the ESI).

In situ detection of piR-651 encased in exosomes
To limit background signals originating from nucleic acids liberated by occasional exosome disruption during ultracentrifugation or from proteins that co-sediment with vesicles, MCF-7 exosomes (ranging from 0 to 5.0×10^8 particles/μL) underwent stepwise pretreatment. This consisted of incubation with 0.1 mg/mL proteinase K at 37°C for 30 min to break down proteins and RNA-protein assemblies, followed by quenching with 5 mM PMSF at room temperature for 20 min, and subsequent digestion of exposed RNAs with 5 U/mL RNase A at 37°C for 30 min. After these steps, 1 nM piR-651 probe was introduced, and incubation continued at room temperature in the dark for 2 h. Fluorescence emission at 665 nm (with 640 nm excitation) was quantified on a multifunctional microplate reader. The signal-to-background ratio (S/B) was then plotted relative to exosome concentration. Comparable assays were executed using the classical piR-651 nanoflare probe and the piR-16926 negative control probe under the same conditions.

Diagnosis of breast cancer by plasma exosomal piR-651 detection
Plasma specimens (40 μL aliquots) obtained from 21 individuals diagnosed with breast cancer and 22 healthy donors were processed following the pretreatment protocol. Each sample then received 1 nM piR-651 probe and was incubated at room temperature for 2 h. A parallel blank sample was prepared by treating 40 μL PBS identically. Fluorescence intensity in all solutions was measured using a multifunctional microplate reader (excitation 640 nm, emission 665 nm). Diagnostic utility was evaluated through scatter plots and receiver operating characteristic (ROC) curve analysis.

Imaging of piR-651 in live cells by piR-651 probe
Cytotoxicity of the piR-651 probe on MCF-7 cells was initially assessed. Around 5000 MCF-7 cells were plated per well in 96-well plates and allowed to adhere for 24 h at 37°C with 5% CO_2. The medium was replaced with 100 μL fresh medium containing 8 μL piR-651 probe, followed by incubation for varying durations (0 to 24 h). At designated time points, medium was removed, cells were exposed to 10-fold diluted MTT reagent for 4 h, and the resulting formazan crystals were dissolved in 100 μL DMSO. Absorbance was recorded at 492 nm with a microplate reader, and cell viability was expressed as a function of incubation time. Equivalent MTT assays examined the effects of AuNPs and the piR-651 probe on MCF-10A cells after 24 h exposure.
For fluorescence imaging studies, MCF-7 or MCF-10A cells were seeded at approximately 5000 cells per confocal dish and cultured for 24 h. Dishes were then supplemented with 0.5 nM piR-651 probe and incubated at 37°C for 0.5–4 h. Hoechst 33342 dye (500 μL) was added for nuclear staining during the final 20 min. After three PBS washes, fresh medium was added, and live cells were visualized under an inverted confocal laser scanning microscope (CLSM). Imaging experiments with the negative control piR-16926 probe in MCF-7 cells followed an analogous workflow.
Further CLSM imaging was conducted on MCF-7 cell variants with either elevated or reduced piR-651 levels, alongside untreated control cells. Three confocal dishes were seeded with ~5000 cells and grown to 70%–80% confluence. Two dishes were transfected with 300 nM piR-651 analog or antisense oligonucleotides using Lipo-8000 reagent. After 2 h, the transfection medium was removed and cells were rinsed three times with PBS. All dishes were subsequently incubated with 0.5 nM piR-651 probe at 37°C for 3 h, followed by Hoechst staining and CLSM observation using the standard imaging protocol.

Results and Discussion

Design and detection principle of the piR-651 probe
To achieve effective in situ recognition of large PIWI-bound piRNA assemblies within exosomes, we constructed a spherical nucleic acid probe utilizing 13-nm gold nanoparticles (AuNPs) as the core, referred to as the piR-651

probe (Scheme 1). The AuNP surface is functionalized with double-stranded DNA duplexes consisting of Anchor DNA and Report DNA components **(Table 1)**. Anchor DNA strands are anchored to the gold core via a 3′ thiol group forming strong Au-S linkages. Each Report DNA functions as an antisense strand specific to piR-651 and is labeled with Cy5 fluorophore at the 5′ position, allowing partial hybridization with the Anchor DNA. In the assembled probe, fluorescence from the Cy5 labels remains strongly suppressed owing to their nearness to the quenching gold surface. Target piR-651 triggers strand displacement through formation of fully matched duplexes with the Report DNA, causing detachment of the labeled strands. The freed Cy5 molecules then emit bright fluorescence signals upon excitation, with emission intensity directly proportional to target abundance.

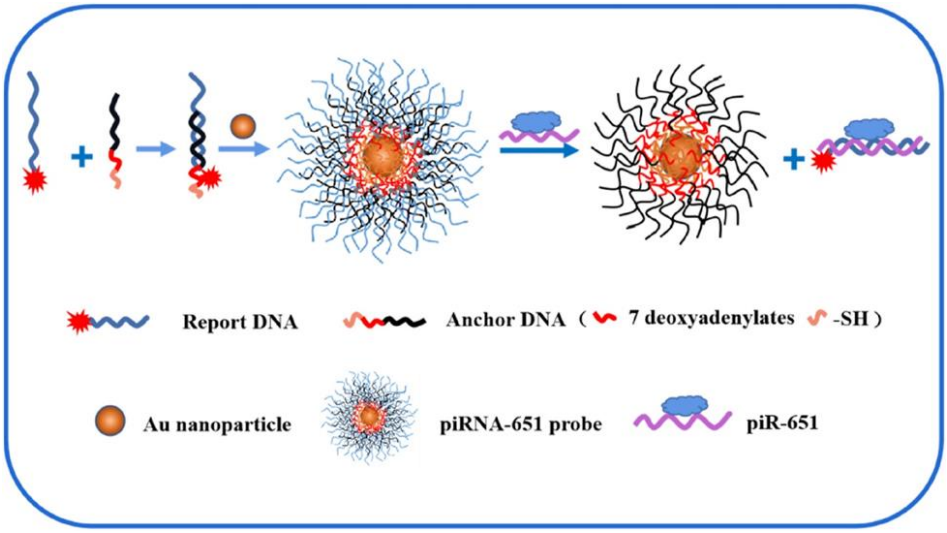

Scheme 1. Structure and detection scheme of the piR-651 probe.

The probe design and sensing strategy differ notably from conventional nanoflare systems. In the standard piR-651 nanoflare, capture DNAs **(Table 1)** are fully complementary to the target. Binding produces longer, more stable hybrids that displace shorter Report strands and restore fluorescence. However, piRNAs naturally exist in complex with 97 kDa PIWI proteins. Progressive attachment of these voluminous complexes to capture sequences causes surface overcrowding on the nanoflare, generating steric constraints that hinder additional binding events and reduce both reaction rate and sensitivity. In the piR-651 probe, target hybridization leads to progressive clearance of Report DNAs from the gold surface, thereby increasing available space and promoting efficient subsequent reactions **(Scheme 1)**.

Synthesis and characteristics of the piR-651 probe

The piR-651 probe was fabricated by the butanol dehydration procedure. Optical characterization began with UV-visible spectroscopy to compare the probe with bare AuNPs. As presented in **Figure 1a**, the plasmon resonance maximum shifted from 519 nm (AuNPs) to 524 nm (piR-651 probe), indicating successful surface modification and increased particle diameter. An additional peak at 645 nm, absent in the AuNP spectrum, confirmed attachment of Cy5-labeled Report DNA. Probe and AuNP concentrations were calculated as 6.7 nM and 10 nM, respectively, based on absorbance values, dilution factors, and the Beer-Lambert law ($\varepsilon = 2.7 \times 10^8$ L mol^{-1} cm^{-1}). Dynamic light scattering showed average hydrated sizes of 41.43 nm for the probe and 14.88 nm for AuNPs **(Figure 1b)**, both with narrow distributions (polydispersity indices 0.282 and 0.178). The piR-651 probe exhibited a markedly more negative Zeta potential than unmodified AuNPs **(Figure 1c)**, verifying dense attachment of negatively charged DNA. TEM analysis revealed well-dispersed spherical particles with uniform size for both AuNPs **(Figure 1d)** and the piR-651 probe **(Figure 1e)**. Measurement of 275 particles yielded a mean AuNP core diameter of 13.18 ± 0.98 nm **(Figure 1f)**.

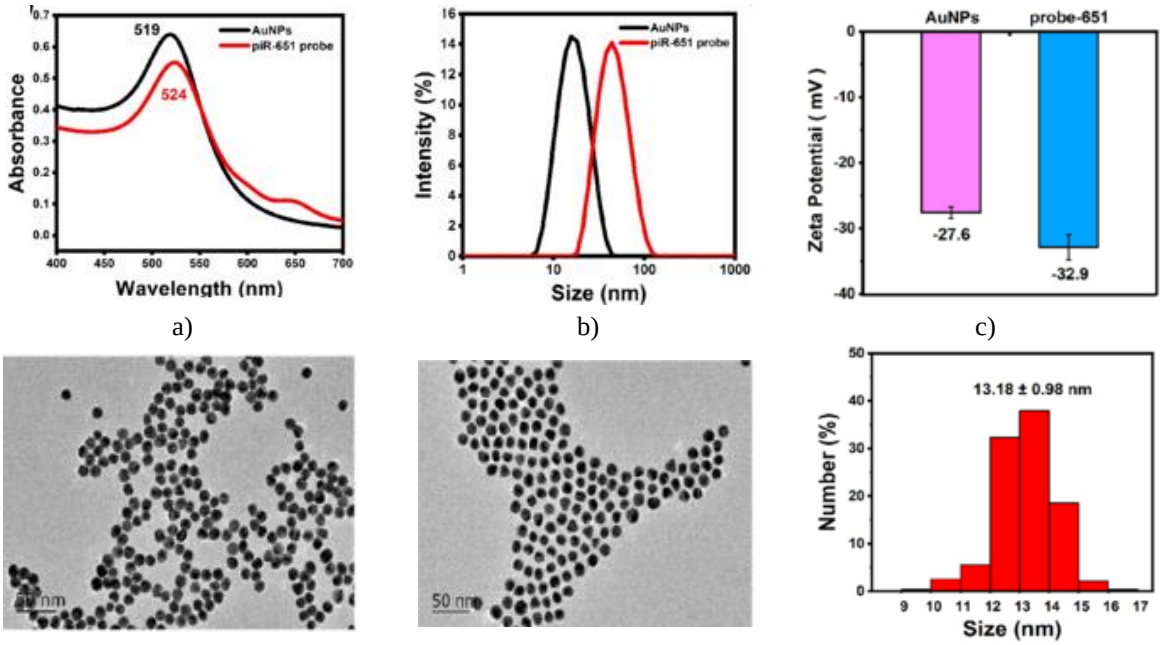

Figure 1. Structural characterization of Au nanoparticles (AuNPs) and the piR-651 probe. (a) UV-visible spectra of the sol of AuNPs and the piR-651 probe. (b) Particle size distribution of AuNPs and piR-651 probe determined by dynamic light scattering. (c) Zeta potential distribution plots for the AuNPs and piR-651 probe. (d) Transmission electron microscopy (TEM) image of AuNPs. (e) TEM image of the piR-651 probe. (f) Size distribution histogram of AuNPs (n = 275) counted from TEM images.

Nucleic acid loading was quantified using the standard addition method. The calibration curve intersected the background fluorescence level at −36.72 nM, corresponding to 36.72 nM duplexes associated with 0.5 nM probe, equivalent to an average of 73 duplex pairs per particle. Synthesis relied on the rapid "flash" butanol dehydration technique pioneered by Deng's group [28], known for its speed, efficiency, and high reproducibility. Compared with an earlier miR-1246 probe prepared via the freezing approach [24], the current construct achieved nearly twice the oligonucleotide density, demonstrating the enhanced loading capacity of the butanol dehydration method and matching prior findings by Deng and colleagues.

Detection performance in buffer and anti-DNase stability of the piR-651 probe

Initial experiments examined the time-dependent response of the piR-651 probe toward its target in HEPES buffer. **Figure 2a** reveals a fast reaction profile, with fluorescence intensity rising sharply during the first 60 min. Consequently, all quantitative assays were performed by incubating 0.5 nM probe with target sequences at room temperature for 1 h. The probe produced a highly linear signal increase across 0–30 nM piR-651 ($R^2 = 0.9993$), as shown in **Figure 2b**. The sensitivity corresponded to 1.12 folds per nM, yielding a limit of detection of 178 pM (determined as 3σ/sensitivity). Signal saturation occurred beyond 30 nM target, aligning with the estimated loading of roughly 73 Report DNA strands per probe particle.

Probe specificity was tested against DNA mimics of miR-21 and miR-1246, plus three random sequences containing 1, 2, or 3 base mismatches relative to piR-651 **(Table 2)**. At 20 nM concentration, the 0.5 nM probe generated a strong response exclusively to the matched target while showing only marginal signals for the other nucleic acids **(Figure 2c)**. This demonstrates excellent selectivity, minimizing interference from co-existing sequences such as miR-21 and miR-1246 commonly found in MCF-7 exosomes.

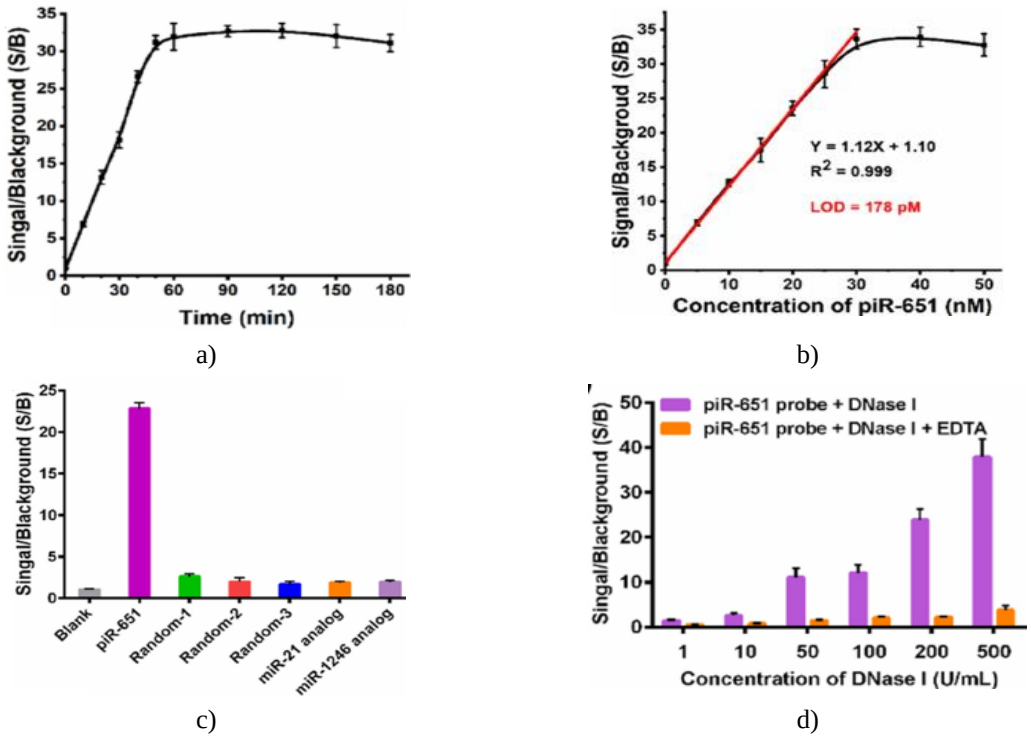

Figure 2. Detection performance and anti-DNase stability of the piR-651 probe in buffer solution. (a) Kinetic curve of piR-651 detection. (b) Standard curve of the quantitative measurement of piR-651. (c) Selective detection of the probe to different nucleic acids. (d) Anti-DNase I stability of piR-651 probe in the presence/absence of EDTA.

Plasma contains high levels of nucleases capable of degrading DNA-based probes and generating false-positive readings. To evaluate resistance, 0.5 nM piR-651 probe was incubated with DNase I (0–500 U/mL) for 1 h. As presented in **Figure 2d**, fluorescence began to increase at 10 U/mL DNase I due to cleavage of surface-bound duplexes and release of Cy5-labeled strands from the gold quencher. Higher enzyme concentrations caused progressively greater degradation. Notably, addition of 1.5 mg/mL EDTA conferred strong protection; even at 500 U/mL DNase I the probe exhibited minimal degradation and negligible nonspecific signal. Because EDTA is the standard anticoagulant used in plasma collection for cancer biomarker studies, the piR-651 probe is compatible with direct analysis of clinical plasma specimens.

Performance of piR-651 probe for in situ detection of cell piR-651

One notable property of gold nanoparticles bearing spherical nucleic acids is their efficient uptake by cells, allowing direct interaction with intracellular molecules. Exploiting this feature, the piR-651 probe was utilized to perform live-cell imaging studies that reveal differences in piR-651 abundance between breast cancer and normal breast epithelial cells. After establishing that the probe displayed low cytotoxicity in both MCF-7 and MCF-10A cell lines, confocal laser scanning microscopy (CLSM) images were acquired for MCF-7 cells exposed to the piR-651 probe or the control piR-16926 probe. The substantial contrast in fluorescence intensity demonstrated specific detection of endogenous piR-651 by the designed probe.

Additional validation involved two MCF-7 derivatives with artificially increased and decreased piR-651 expression. Following 3 h incubation with the probe, CLSM imaging **(Figure 4)** showed clear gradations in red fluorescence, progressing from weak in the down-regulated cells to intense in the up-regulated cells. This pattern verifies the probe's effectiveness for in situ monitoring and differentiation of piR-651 levels inside living cells.

Time-resolved imaging experiments indicated steadily increasing Cy5 fluorescence in MCF-7 cells during 0.5–4 h exposure to the probe **(Figure 3a)**. By comparison, MCF-10A normal cells produced consistently faint signals across the same intervals **(Figure 3b)**. The data therefore support higher piR-651 expression in cancerous MCF-7 cells than in normal MCF-10A cells, aligning with previous observations [17].

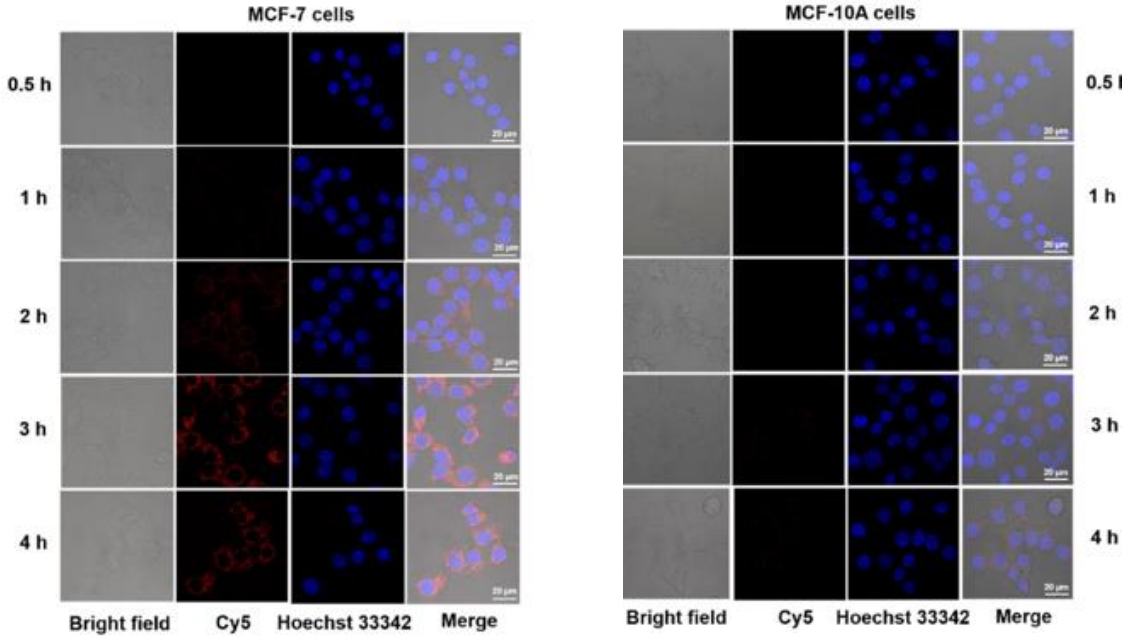

a) b)

Figure 3. Confocal laser scanning microscopic imaging of MCF-7 cells (a) and MCF-10A cells (b) after incubation with the piR-651 probe for 0.5, 1, 2, 3, and 4 h, respectively.

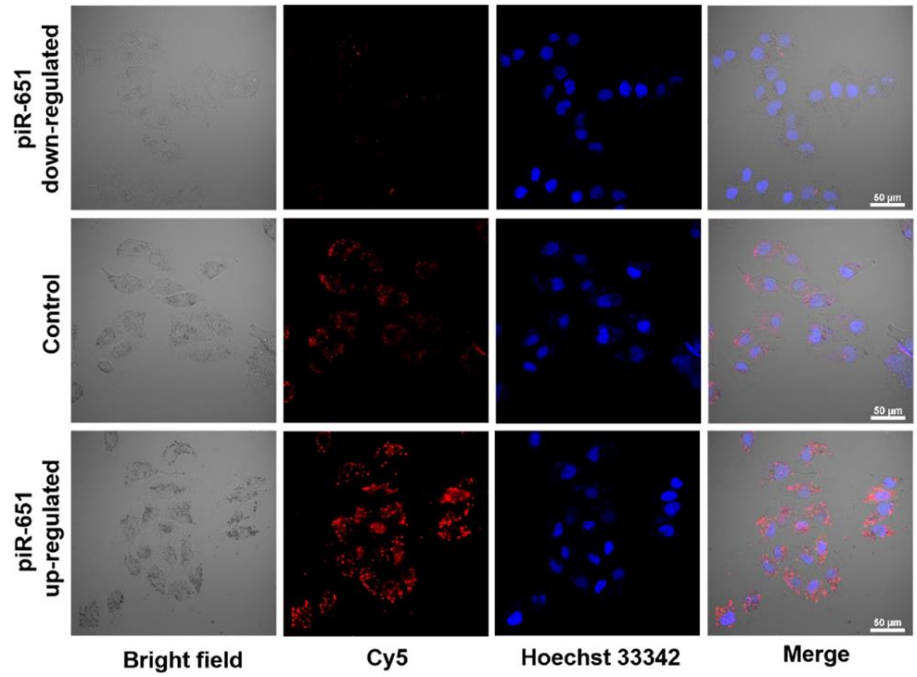

Figure 4. Confocal laser scanning microscopic imaging of three MCF-7 cell lines after incubation with the piR-651 probe for 3 h. From the top row to the bottom row: MCF-7 cells with their inner piR-651 down-regulated, control, and up-regulated.

Performance of piR-651 probe for in situ detection of exosomal piR-651

Before assessing the probe's capability to detect piR-651 inside exosomes, the identity of vesicles collected from MCF-7 cell culture was confirmed. Nanoparticle tracking analysis (NTA) showed that 80% of particles measured between 45 and 195 nm, with mean and median diameters of 153.3 nm and 138.1 nm, respectively **(Figure 5a)**. This size range is characteristic of exosomes, and the total concentration in 100 µL PBS was 1.4×10^9 particles/µL. TEM visualization confirmed the presence of membrane-enclosed vesicles with typical rounded morphology **(Figure 5b)**. Western blot results identified the exosomal markers CD63 and TSG101 **(Figure 5c)**, matching

known exosome protein signatures [30]. These characterizations establish that the isolated vesicles are bona fide exosomes suitable as a model system for testing the piR-651 probe.

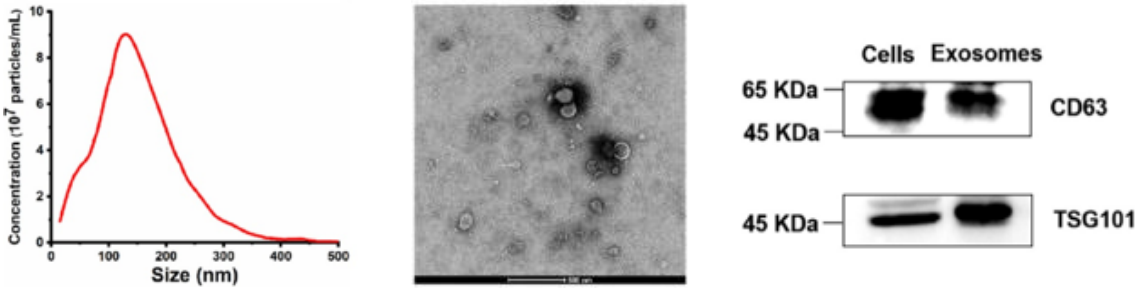

a) b) c)

Figure 5. Characterization of exosomes secreted by MCF-7 cells.
(a) Particle size distribution map of exosomes at 3000-fold dilution measured by nanoparticle tracking analyzer. (b) TEM image of exosomes. Scale bar: 500 nm. (c) Western blotting of the characteristic proteins of MCF-7 cells and their secreted exosomes.

In situ detection of piR-651 within exosomes

Our earlier work demonstrated that nucleic acid probes can produce false-positive signals through unintended interactions with non-exosomal contaminants. To confirm genuine in situ detection of piR-651 inside exosomes, we examined whether the piR-651 probe was similarly susceptible to such interference. MCF-7 exosomes were incubated with the piR-651 probe after being left untreated or pretreated with proteinase K and RNase A, and the resulting fluorescence intensities were compared. Untreated exosomes generated stronger signals than the pretreated samples, mirroring observations previously reported for Au nanoflare and molecular beacon systems [24, 31]. Notably, the magnitude of false-positive signals from the piR-651 probe interacting with untreated exosomes was considerably greater. This outcome likely stems from the extended Report DNAs-Anchor DNAs segments on the piR-651 probe—longer than the Report-Capture DNAs used in miRNA-targeted nanoflares—which facilitate greater non-specific associations with proteins and RNAs liberated from compromised EVs during ultracentrifugation. Such binding promotes dissociation of the Report DNA, leading to artifactual signals. Hence, exosome pretreatment following the International Society for Extracellular Vesicles guidelines is indispensable in all ensuing EV-related experiments to eliminate extraneous false-positive contributions from outside the vesicles.

Subsequently, the temporal profile of exosomal piR-651 detection with the piR-651 probe was characterized. Fluorescence intensity rose steadily during incubation, becoming significantly distinguishable from background after 30 min and attaining peak levels near 2 h. Probe responses were therefore quantified after 2 h co-incubation with MCF-7 exosomes across a range of concentrations. The signal-to-blank (S/B) ratio displayed a clear positive correlation with EV concentration, corresponding to an estimated detection limit of 5×10^7 particles/μL **(Figure 6a)**. At 5×10^8 particles/μL, the S/B ratio reached 17.03, underscoring the probe's strong responsiveness. **Figure 6a** additionally reveals concentration-dependent signals from EVs secreted by normal breast cells (MCF-10A), albeit with substantially weaker intensities than those elicited by equivalent numbers of MCF-7 EVs. This pattern is consistent with the differing piR-651 abundance between the two exosome types, as previously established by RT-qPCR [21].

To substantiate that the signals derived specifically from intravesicular piR-651, a negative control probe directed against piR-16926 was generated and tested in parallel with MCF-7 exosomes. As observed in cellular imaging, signals from the piR-16926 probe showed little dependence on EV concentration and stayed markedly below those of the piR-651 probe **(Figure 6b)**. This agrees with next-generation sequencing data indicating far lower piR-16926 expression relative to piR-651 in MCF-7 exosomes. Collectively, these findings confirm that fluorescence from both probes results from sequence-specific recognition of their target piRNAs, rather than non-specific interactions with external proteins or impurities.

Additional evidence for in situ detection of piR-651 inside EVs came from super-resolution optical microscopy and transmission electron microscopy analyses performed after incubating the piR-651 probe with MCF-7 EVs. In **Figure 6d**, PKH67-stained EVs exhibited green fluorescence, while release of the Cy5-labeled reporter produced red fluorescence. Overlap of the red and green signals in merged images indicated that probe activation

occurred primarily within the vesicle interior. TEM observations **(Figure 6e)** further confirmed probe internalization into EVs following 2 h incubation. Internalization was variable: certain EVs remained unlabeled, while others contained between 3 and 8 probes.

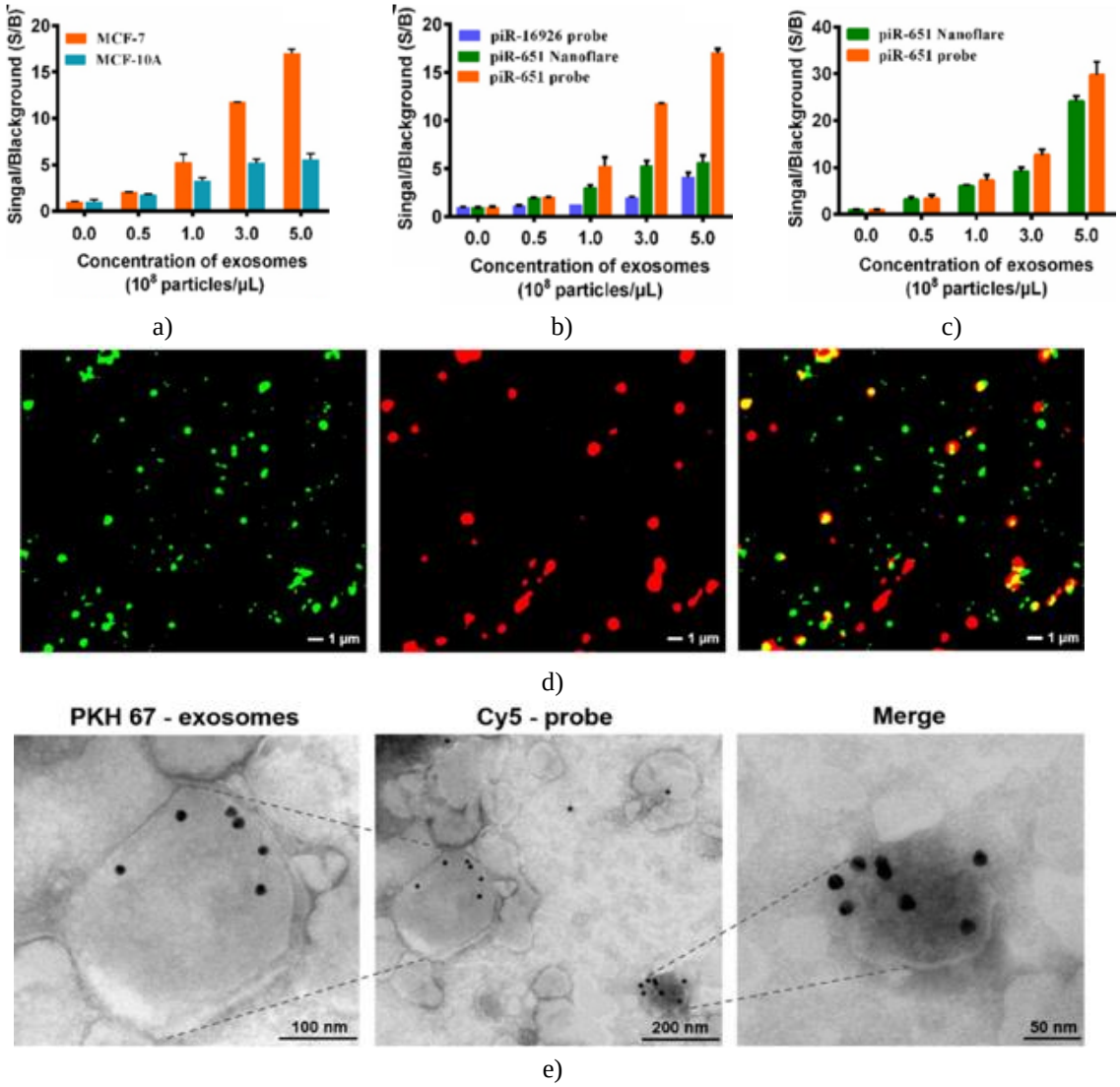

Figure 6. In situ detection of piR-651 in exosomes.
(a) Quantitative fluorescence responses of the piR-651 probe toward MCF-7 and MCF-10A exosomes. (b) Quantitative fluorescence responses of the piR-651 probe, piR-16926 probe, and piR-651 Nanoflare with MCF-7 exosomes. (c) Quantitative responses of the piR-651 probe and piR-651 Nanoflare to Triton X-100 and proteinase K-treated MCF-7 exosomes. (d) Super-resolution optical microscopy images (SIM mode) of MCF-7 exosomes incubated with the piR-651 probe. Scale bar: 1 μm. Left: PKH67 channel. Center: Cy5 channel. Right: Merged image. (e) TEM images of piR-651 probe internalization in MCF-7 exosomes after co-incubation. Scale bars: 200, 100, and 50 nm (left to right).

To evaluate whether the piR-651 probe architecture circumvents steric constraints imposed by PIWI protein–RNA complexes, a standard Nanoflare version of the piR-651 probe (piR-651 Nanoflare; Table 1) was prepared. When tested in solution against a protein-free piR-651 DNA analog, the sensitivity and detection limit of the piR-651 Nanoflare closely resembled those of the original piR-651 probe **(Figure 2b)**. In contrast, the piR-651 probe demonstrated markedly superior sensitivity when detecting piR-651 in intact MCF-7 EVs **(Figure 6b)**. To clarify whether this difference arose from distinct detection mechanisms linked to probe structure, MCF-7 EVs were lysed with Triton X-100 and treated with proteinase K to disassemble PIWI protein–RNA complexes, after which both probes were applied. Under these conditions, the two probes produced nearly identical fluorescence signals **(Figure 6c)**. Because the fundamental designs and fluorophore modifications are comparable, the probes are

expected to exhibit similar uptake efficiencies into MCF-7 EVs. Thus, the enhanced performance of the piR-651 probe in native exosomes indicates that its specialized configuration successfully bypasses steric hindrance from bulky PIWI protein–RNA assemblies, resulting in improved detection sensitivity.

Utilization of the piR-651 probe for breast cancer diagnosis

Earlier research has established that piR-651 levels are markedly elevated in breast cancer tissues, malignant cells, and circulating extracellular vesicles when compared with corresponding normal samples, where it actively drives cancer cell proliferation and migration [18, 32]. These observations highlight piR-651 as a valuable candidate biomarker for breast cancer detection. Capitalizing on the capacity of the piR-651 probe to quantify intravesicular piR-651 content, we implemented the probe in a liquid biopsy strategy focused on the in situ identification of this piRNA in plasma-derived extracellular vesicles from peripheral blood specimens.

Following mild pretreatment of plasma specimens from breast cancer patients (n = 21) and healthy volunteers (n = 22) using proteinase K and RNase A, the piR-651 probe was applied to assess piR-651 abundance within the plasma exosomes. Analysis of the signal-to-background (S/B) ratios yielded mean values of 11.06 ± 1.86 (mean ± SD) for the patient cohort and 6.88 ± 1.53 (mean ± SD) for the control group. A t-test demonstrated a highly significant difference between the average fluorescence intensities of the two groups ($p < 0.0001$) **(Figure 7a)**. Receiver operating characteristic (ROC) curve evaluation **(Figure 7b)** determined that an optimal S/B threshold of 9.193 provided 85.7% sensitivity and 100% specificity for breast cancer classification. The area under the curve (AUC) reached 0.9913, denoting outstanding diagnostic precision.

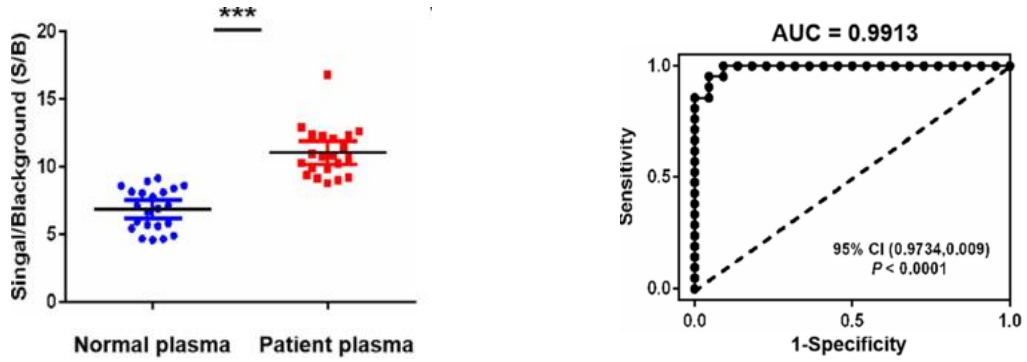

a) b)

Figure 7. Liquid biopsy approach for breast cancer diagnosis via detection of piR-651 in plasma exosomes using the piR-651 probe.

(a) Scatter plot of fluorescence signals generated by the piR-651 probe in plasma samples from breast cancer patients (n = 21) and normal controls (n = 22). $p < 0.0001$. (b) Receiver operating characteristic (ROC) curves constructed from S/B ratios for distinguishing between groups.

The present study describes the development of an innovative spherical gold nanoprobe tailored for the in situ detection of piRNAs inside extracellular vesicles. Compared with a traditional nanoflare design, the piR-651 probe achieved considerably superior sensitivity. This improvement arises from the specific architecture of the Anchor-Report DNA components and the underlying detection process, which successfully bypasses escalating steric barriers encountered when targeting piR-651 complexed with large PIWI protein–RNA assemblies. The conceptual framework employed here holds promise for extension to other biosensing platforms designed for sizable molecular targets. Utilizing this probe, we implemented a convenient and reliable liquid biopsy technique that enables direct detection of the key biomarker piR-651 within plasma extracellular vesicles, supporting accurate breast cancer diagnosis. The probe is also suitable for real-time imaging of piRNAs in living cells.

Conclusion

In conclusion, this research introduces an effective strategy for the in situ monitoring of piRNAs in both cellular and exosomal environments, paving the way for future applications in cancer molecular diagnostics and gene therapy investigations.

Acknowledgments: None

Conflict of Interest: None

Financial Support: None

Ethics Statement: None

References

1. International Agency for Research on Cancer. Global cancer burden growing, amidst mounting need for services. Saudi Med J. 2024;45(3):326-7.
2. Wellings E, Vassiliades L, Abdalla R. Breast Cancer Screening for High-Risk Patients of Different Ages and Risk - Which Modality Is Most Effective? Cureus. 2016;8(12):e945.
3. Nikanjam M, Kato S, Kurzrock R. Liquid biopsy: current technology and clinical applications. J Hematol Oncol. 2022;15(1):131.
4. Alix-Panabières C, Pantel K. Liquid Biopsy: From Discovery to Clinical Application. Cancer Discov. 2021;11(4):858-73.
5. Ignatiadis M, Sledge GW, Jeffrey SS. Liquid biopsy enters the clinic - implementation issues and future challenges. Nat Rev Clin Oncol. 2021;18(5):297-312.
6. Pinzani P, D'Argenio V, Del Re M, Pellegrini C, Cucchiara F, Salvianti F, et al. Updates on liquid biopsy: current trends and future perspectives for clinical application in solid tumors. Clin Chem Lab Med. 2021;59(7):1181-90.
7. Kalluri R, LeBleu VS. The biology, function, and biomedical applications of exosomes. Science. 2020;367(6477):eaau6977.
8. Lai JJ, Chau ZL, Chen SY, Hill JJ, Korpany KV, Liang NW, et al. Exosome Processing and Characterization Approaches for Research and Technology Development. Adv Sci (Weinh). 2022;9(5):2103222.
9. Girard A, Sachidanandam R, Hannon GJ, Carmell MA. A germline-specific class of small RNAs binds mammalian Piwi proteins. Nature. 2006;442(7099):199-202.
10. Grivna ST, Beyret E, Wang Z, Lin H. A novel class of small RNAs in mouse spermatogenic cells. Genes Dev. 2006;20(13):1709-14.
11. Watanabe T, Takeda A, Tsukiyama T, Mise K, Okuno T, Sasaki H, et al. Identification and characterization of two novel classes of small RNAs in the mouse germline: retrotransposon-derived siRNAs in oocytes and germline small RNAs in testes. Genes Dev. 2006;20(13):1732-43.
12. Ozata DM, Gainetdinov I, Zoch A, O'Carroll D, Zamore PD. PIWI-interacting RNAs: small RNAs with big functions. Nat Rev Genet. 2019;20(2):89-108.
13. Ku HY, Lin H. PIWI proteins and their interactors in piRNA biogenesis, germline development and gene expression. Natl Sci Rev. 2014;1(2):205-18.
14. Czech B, Munafò M, Ciabrelli F, Eastwood EL, Fabry MH, Kneuss E, et al. piRNA-Guided Genome Defense: From Biogenesis to Silencing. Annu Rev Genet. 2018;52:131-57.
15. Lin Y, Zheng J, Lin D. The role of PIWI-interacting RNAs in cancer: signaling pathways and clinical implications. Semin Cancer Biol. 2020;104:111-22.
16. Maleki Dana P, Mansournia MA, Mirhashemi SM. PIWI-interacting RNAs: new biomarkers for diagnosis and treatment of cancer. Cell Biosci. 2020;10:44.
17. Liu Y, Dou M, Song X, Dong Y, Liu S, Liu H, et al. The emerging role of the piRNA/piwi complex in cancer. Mol Cancer. 2019;18(1):123.
18. Liu T, Wang J, Sun L, Li M, He X, Jiang J, et al. PIWI-interacting RNA-004800 is regulated by proliferation and serves as a novel prognostic biomarker in pancreatic cancer. Cell Cycle. 2021;20(15-16):1603-17.
19. Lee YJ, Moon SU, Park MG, Jung WY, Park YK, Song SK, et al. A novel DNA-binding protein, Php, activates piRNA transcription in Drosophila. Biomaterials. 2016;101:143-55.
20. Jia R, He X, Ma W, Lei Y, Cheng H, Sun H, et al. Sensitive and Specific Detection of MicroRNA by Dual-Fluorescence and Electrochemical Signal Amplification. Anal Chem. 2019;91(23):15107-13.

21. Zhang LM, Gao QX, Chen J, Li B, Li MM, Zheng L, et al. A label-free fluorescent sensor based on CRISPR-Cas12a and G-quadruplex-thioflavin T for the detection of microRNA. Anal Chim Acta. 2022;1192:339382.
22. Zhang LM, Gao QX, Xie BP, Chen J, Duan WJ. A cascade amplification strategy based on CRISPR-Cas12a and a G-quadruplex DNAzyme for the detection of miRNA-21. Chem Commun (Camb). 2022;58(37):5793-6.
23. Gao QX, Zhang LM, Wu QQ, Guo FF, Chen J, Li MM, et al. A dual-signal amplification strategy based on CRISPR-Cas12a and DNAzyme for ultrasensitive detection of microRNA. Sens Actuators B Chem. 2023;393:134272.
24. Zhai LY, Li MX, Pan WL, Chen Y, Li MM, Pang JX, et al. A Novel Electrochemical Biosensor for MicroRNA Detection Based on a DNA Tetrahedron and a Catalytic Hairpin Assembly. ACS Appl Mater Interfaces. 2018;10(45):39478-86.
25. Li Y, Deng J, Han Z, Liu C, Tian F, Xu R, et al. A DNA Nanodevice for Monitoring MicroRNA-21 in Living Cells. J Am Chem Soc. 2021;143(3):1290-5.
26. Li J, Wang J, Liu S, Xie N, Quan K, Yang Y, et al. A DNAzyme-based logic gate for microRNA detection and imaging in living cells. Angew Chem Int Ed Engl. 2020;59(45):20104-11.
27. Liu J, Lu Y. A colorimetric lead biosensor using DNAzyme-directed assembly of gold nanoparticles. Nat Protoc. 2006;1(1):246-52.
28. Hao Y, Li YJ, Song L, Deng ZX. A DNAzyme-Based Fluorescent Biosensor for Copper Ions in Living Cells. J Am Chem Soc. 2021;143(8):3065-9.
29. Seferos DS, Giljohann DA, Hill HD, Prigodich AE, Mirkin CA. Nano-flares: probes for transfection and mRNA detection in living cells. J Am Chem Soc. 2007;129(50):15477-9.
30. Purushothaman A. Isolation and Characterization of Exosomes from Cancer Cells. In: Vigetti D, Theocharis AD, editors. The Extracellular Matrix. Vol. 1952. New York, NY: Humana Press; 2019. p. 233-44.
31. Chen Y, Zhai LY, Zhang LM, Ma XS, Liu Z, Li MM, et al. An electrochemical biosensor for the detection of microRNA-21 based on a DNA tetrahedron and a catalytic hairpin assembly. Analyst. 2021;146(7):2264-71.
32. Maleki Dana P, Mansournia MA, Mirhashemi SM. PIWI-interacting RNAs: new biomarkers for diagnosis and treatment of cancer. Cell Biosci. 2020;10:44.